LUND UNIVERSITY

Calculation of antenna radiation center using angular momentum

Friden, Jonas; Kristensson, Gerhard

2012

Link to publication

Citation for published version (APA):
Friden, J., & Kristensson, G. (2012). *Calculation of antenna radiation center using angular momentum*. (Technical Report LUTEDX/(TEAT-7219)/1-21/(2012); Vol. TEAT-7219). The Department of Electrical and Information Technology.

Total number of authors:
2

General rights
Unless other specific re-use rights are stated the following general rights apply:
Copyright and moral rights for the publications made accessible in the public portal are retained by the authors and/or other copyright owners and it is a condition of accessing publications that users recognise and abide by the legal requirements associated with these rights.
• Users may download and print one copy of any publication from the public portal for the purpose of private study or research.
• You may not further distribute the material or use it for any profit-making activity or commercial gain
• You may freely distribute the URL identifying the publication in the public portal

Read more about Creative commons licenses: https://creativecommons.org/licenses/

Take down policy
If you believe that this document breaches copyright please contact us providing details, and we will remove access to the work immediately and investigate your claim.

LUND UNIVERSITY

PO Box 117
221 00 Lund
+46 46-222 00 00

CODEN:LUTEDX/(TEAT-7219)/1-20/(2012)

Revision No. 1: January 2013

Calculation of antenna radiation center using angular momentum

Jonas Fridén and Gerhard Kristensson

Electromagnetic Theory
Department of Electrical and Information Technology
Lund University
Sweden

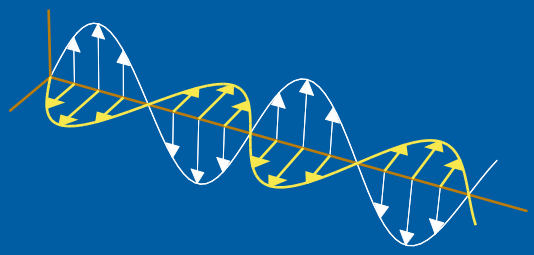

Jonas Fridén
Jonas.Friden@ericsson.com

Ericsson AB
Antennas, Propagation and Deployments
Lindholmspiren 11
417 56 Göteborg
Sweden

Gerhard Kristensson
Gerhard.Kristensson@eit.lth.se

Department of Electrical and Information Technology
Electromagnetic Theory
Lund University
P.O. Box 118
SE-221 00 Lund
Sweden

Editor: Gerhard Kristensson
© Jonas Fridén and Gerhard Kristensson, Lund, October 10, 2012

Abstract

An algorithm to compute the radiation center of an antenna based on the Spherical wave expansion (SWE) is introduced. The method is based on the angular momentum vector that is uniquely defined for any antenna far field pattern. The radiation center is defined as the phase reference point where the angular momentum is minimized and corresponds to minimizing the phase variations in the antenna far field pattern. In addition, this approach also allows for determination of the current distribution axis.

1 Introduction

Accurate calculation of the phase center is instrumental in many antenna applications. When a multi-port antenna is measured, it is valuable to determine the origins of the antenna radiation from each port. This can provide insights into how the antenna currents are set up, improve array synthesis using measured embedded patterns, and investigate the impact of mutual coupling. When a large number of antenna ports are used, it can also serve as a double check on how the connectors maps on the antenna elements. For small antennas, a common concern is whether the intended antenna element radiates, or if it works as a probe setting up currents in the surrounding structures. Retrieval of the origin of the radiation can cast some light also in this area.

According to the IEEE standard 145-1993 [1] the phase center is defined as:

> "**2.270** phase center. The location of a point associated with an antenna such that, if it is taken as the center of a sphere whose radius extends into the far-field, the phase of a given field component over the surface of the radiation sphere is essentially constant, at least over that portion of the surface where the radiation is significant."

Obviously, this definition is intended for use with antennas with a manifest major lobe and with a well-defined co-polarization. For general antennas, this definition of phase center is less useful.

First, it is noted that "essentially constant" is a qualitative measure, and the portion of the main lobe to be used is not defined. For antennas without a distinct main lobe, such as antennas on phones and laptops, the concept of significant directions becomes less relevant. Moreover, the phase center can vary when evaluated for different field components.

The aim of this paper and main questing addressed in this paper is: Is it possible to define a point which coincides with the phase center for antennas with distinct major lobe and co-polarization, and that is useful for a general antenna far field pattern? The answer is affirmative, and the point is uniquely defined. To avoid confusion, this point is called the *radiation center*. In addition, the method provides an equivalent *current distribution axis*.

2 Background and method

The far field amplitude $\boldsymbol{F}(\hat{\boldsymbol{r}})$ is defined as the limit

$$\boldsymbol{F}(\hat{\boldsymbol{r}}) = \lim_{r\to\infty} \sqrt{\frac{4\pi}{\eta_0}} r e^{jkr} \boldsymbol{E}(\boldsymbol{r}) \tag{2.1}$$

with an underlying time convention $\exp(\mathrm{j}\omega t)$. Here, $\eta_0 = \sqrt{\mu_0/\epsilon_0}$ is the vacuum impedance, and $k = 2\pi/\lambda$ is the wave number. Furthermore, the far field amplitude is normalized to 1W radiated power, *e.g.*,

$$\iint_\Omega \boldsymbol{F}^*(\hat{\boldsymbol{r}}) \cdot \boldsymbol{F}(\hat{\boldsymbol{r}}) \mathrm{d}\Omega = 1. \tag{2.2}$$

where the integration is over the unit sphere Ω, and $\mathrm{d}\Omega$ is the surface measure on the unit sphere.

The Spherical wave expansion (SWE) of the far field amplitude $\boldsymbol{F}(\hat{\boldsymbol{r}})$ is denoted

$$\boldsymbol{F}(\hat{\boldsymbol{r}}) = \sum_{\tau=1}^{2} \sum_{l=1}^{\infty} \sum_{m=-l}^{l} a_{\tau lm} \boldsymbol{A}_{\tau lm}(\hat{\boldsymbol{r}}) = \sum_{\tau lm} a_{\tau lm} \boldsymbol{A}_{\tau lm}(\hat{\boldsymbol{r}}), \tag{2.3}$$

where the vector spherical harmonics $\boldsymbol{A}_{\tau lm}(\hat{\boldsymbol{r}})$ are defined in App. A. The mode amplitudes are calculated as

$$a_{\tau lm} = \iint_\Omega \boldsymbol{A}^*_{\tau lm}(\hat{\boldsymbol{r}}) \cdot \boldsymbol{F}(\hat{\boldsymbol{r}}) \mathrm{d}\Omega, \tag{2.4}$$

which by (2.2) are normalized as

$$\sum_{\tau lm} |a_{\tau lm}|^2 = 1.$$

The widely accepted truncation limits in the use of SWEs are [4]

$$\begin{cases} l \le l_{\max} = [k r_{\min}] + n_1, \\ |m| \le m_{\max} = [k \rho_{\min}] + n_2. \end{cases} \tag{2.5}$$

Here, $r_{\min}$ and $\rho_{\min}$ are the radii of the minimum sphere and the minimum cylinder circumscribing all antenna currents, respectively. The minimum sphere is centered at the origin, and the minimum cylinder is a circular cylinder, with symmetry axis through the origin, and along the z-axis. The square brackets denote integer part, k is the wave number, and the integers $n_{1,2}$ are chosen to get a desired numerical accuracy [4, 5]. A common choice is $n_1 = n_2 = 10$.

Clearly, the relation between antenna size and truncation limits provides a means to minimize the mode content, namely by translating and rotating the antenna to minimize $r_{\min}$ and $\rho_{\min}$. However, the truncation limits in (2.5) are discrete functions, and the integers $n_{1,2}$ are non-trivial functions of accuracy. Therefore, they are not well suited for numerical optimization.

A better choice of cost functions, providing continuous measures of the mode contents of the SWE, is the square of the angular momentum L^2 and its squared z-projection L_z^2. By definition, these operations are

$$\begin{cases} L^2 = \sum_{\tau lm} l(l+1)|a_{\tau lm}|^2, \\ L_z^2 = \sum_{\tau lm} m^2|a_{\tau lm}|^2. \end{cases} \tag{2.6}$$

These functions provide continuous measures of mode contents. The origin of these definition is the quantum-mechanical definitions of angular momentum with $\hbar = 1$ [7].

Upon translation of the origin of the far field, it is shown that L^2 has a unique minimum in space. Note that the mode coefficients $a_{\tau lm}$, see (2.4), used to get L^2 and L_z^2, utilize the full sphere patterns of all field components. Hence, all ambiguities in the IEEE definition of the phase center are resolved. The point of minimum of L^2 corresponds to a minimal phase variation in the sense that the far field can be represented with a minimum set of modes, which implicitly minimizes the phase variations of the far field.

Moreover, by rotating the far field and evaluating L_z^2, the current distribution orientation can be characterized. The minimum values of L^2 and L_z^2 can be used to estimate the physical size of the antenna currents. In particular, the quotient

$$s = \sqrt{\frac{\min L_z^2}{\min L^2}} \tag{2.7}$$

is a measure of the sphericity of the antenna current distribution.

Furthermore, the proposed method can be extended to a range of frequencies and/or a number of antenna ports, which generalizes the concept of phase center in a natural way.

3 Angular momentum operators

When using a SWE, it is natural to define the angular momentum functions (2.6) in terms of mode amplitudes $a_{\tau lm}$. However, equivalent expressions can be derived using the far field amplitude $\boldsymbol{F}(\hat{\boldsymbol{r}})$ directly. To do this, angular momentum operators are used. The angular momentum operator is defined as [2, 7]

$$\mathcal{L} = -\mathrm{j}(\boldsymbol{r} \times \nabla). \tag{3.1}$$

Note that $\boldsymbol{\mathcal{L}F}$ is a dyadic quantity, see Appendix A for the spherical coordinate representation. The operators for L^2 and L_z^2 are

$$\begin{cases} \mathcal{L}^2 = \mathcal{L} \cdot \mathcal{L} = -(\boldsymbol{r} \times \nabla) \cdot (\boldsymbol{r} \times \nabla) = -\nabla_\Omega^2, \\ \mathcal{L}_n = \hat{\boldsymbol{n}} \cdot \mathcal{L}, \\ \mathcal{L}_n^2 = (\hat{\boldsymbol{n}} \cdot \mathcal{L})(\hat{\boldsymbol{n}} \cdot \mathcal{L}), \end{cases} \tag{3.2}$$

where the angular part of the Laplace operator in terms of spherical coordinates reads

$$\nabla_\Omega^2 = \frac{1}{\sin\theta}\frac{\partial}{\partial\theta}\left(\sin\theta\frac{\partial}{\partial\theta}\right) + \frac{1}{\sin^2\theta}\frac{\partial^2}{\partial\phi^2}.$$

In the z-direction we get in spherical coordinates

$$\mathcal{L}_z = -\mathrm{j}\frac{\partial}{\partial\phi}.$$

For the purposes of this work, it's useful to complement the angular momentum operator on a transverse vector field with a projection $\mathcal{P}_\Omega$ on the directions transverse to $\hat{\boldsymbol{r}}$. The vector spherical harmonics corresponding to $\tau = 1, 2$ are eigenstates of $\mathcal{P}_\Omega\mathcal{L}^2$ and $\mathcal{L}_z$ and the relations read [6, pp. 1900–01] and Appendix A

$$\begin{cases} \mathcal{P}_\Omega\mathcal{L}^2\boldsymbol{A}_{\tau lm} = l(l+1)\boldsymbol{A}_{\tau lm}, \\ \mathcal{L}_z(\hat{\boldsymbol{\theta}}\cdot\boldsymbol{A}_{\tau lm}) = m(\hat{\boldsymbol{\theta}}\cdot\boldsymbol{A}_{\tau lm}), \\ \mathcal{L}_z(\hat{\boldsymbol{\phi}}\cdot\boldsymbol{A}_{\tau lm}) = m(\hat{\boldsymbol{\phi}}\cdot\boldsymbol{A}_{\tau lm}). \end{cases}$$

By expanding the far field amplitude $\boldsymbol{F}$ in a SWE (2.3), and using (A.2), it then follows that

$$L^2 = \iint_\Omega \boldsymbol{F}(\hat{\boldsymbol{r}})^*\cdot\mathcal{P}_\Omega\mathcal{L}^2\boldsymbol{F}(\hat{\boldsymbol{r}})\mathrm{d}\Omega = \iint_\Omega \boldsymbol{F}(\hat{\boldsymbol{r}})^*\cdot\mathcal{L}^2\boldsymbol{F}(\hat{\boldsymbol{r}})\mathrm{d}\Omega. \tag{3.3}$$

For L_z^2 the following expression is used

$$L_z^2 = \iint_\Omega \left[(\mathcal{L}_zF_\theta)^*(\mathcal{L}_zF_\theta) + (\mathcal{L}_zF_\phi)^*(\mathcal{L}_zF_\phi)\right]\mathrm{d}\Omega. \tag{3.4}$$

4 Properties of angular momentum

In classical mechanics angular momentum is defined as $\boldsymbol{L} = \sum_i \boldsymbol{r}_i\times\boldsymbol{p}_i$. It has the following properties:

1. $|\boldsymbol{L}|$ is conserved under rotations.
2. $L_z = \boldsymbol{L}\cdot\hat{\boldsymbol{z}}$ is conserved under translations along $\hat{\boldsymbol{z}}$. (Hint: let $\boldsymbol{r}_i \mapsto \boldsymbol{r}_i - z\hat{\boldsymbol{z}}$)
3. $L^2 = \boldsymbol{L}\cdot\boldsymbol{L}$ is a quadratic form
$$\boldsymbol{L}\cdot\boldsymbol{L} \mapsto \boldsymbol{L}\cdot\boldsymbol{L} - 2\boldsymbol{d}\cdot(\boldsymbol{p}\times\boldsymbol{L}) + \boldsymbol{d}\cdot\left(\mathbf{I}|\boldsymbol{p}|^2 - \boldsymbol{p}\boldsymbol{p}\right)\cdot\boldsymbol{d},$$
in the translation vector $\boldsymbol{d}$. Here $\boldsymbol{p} = \sum\boldsymbol{p}_i$. (Hint: let $\boldsymbol{r}_i \mapsto \boldsymbol{r}_i - \boldsymbol{d}$).
4. L_z changes under rotations.

These properties also hold for L^2 and L_z^2 as defined in (2.6). The invariants 1 and 2 follow from the basic rotation and translation properties of the SWE outlined in Sections 4.1 and 4.2, see also [4]. The translational and rotational behavior of L^2 and L_z^2 are outlined in Sections 4.3 and 4.4.

4.1 Invariants under rotations

Let $\mathcal{R}(\alpha,\beta,\gamma)$ be a zyz Euler rotation operator applied to the far field. The z-axis rotations only shift the phase of the mode amplitudes $a_{\tau lm}$, and thus both L^2 and L_z^2 are unchanged. A y-axis rotation shifts the m-indices, but do not mix the l-indices [4, (A 2.2)]. Explicitly,

$$\mathcal{R}(0,\beta,0)\boldsymbol{A}_{\tau lm}(\hat{\boldsymbol{r}}) = \sum_{m'=-l}^{l} d^l_{mm'}(\beta)\boldsymbol{A}_{\tau lm'},$$

where the real coefficients $d^l_{mm'}(\beta)$ satisfy [3]

$$\sum_{m''=-l}^{l} d^l_{m''m}(\beta)d^l_{m''m'}(\beta) = \delta_{mm'}.$$

Note that the summation is only over the m-indices. The mode coefficients are transformed as

$$a_{\tau lm}(\beta) = \sum_{m'=-l}^{l} d^l_{mm'}(\beta)a_{\tau lm'}$$

which leads to

$$\begin{aligned}
&\sum_m |a_{\tau lm}(\beta)|^2 = \\
&\sum_m\sum_{m'}\sum_{m''} d^l_{mm'}(\beta)d^l_{mm''}(\beta)a^*_{\tau lm'}a_{\tau lm''} = \\
&\sum_{m'}\sum_{m''} \delta_{m'm''}a^*_{\tau lm'}a_{\tau lm''} = \sum_{m'} |a_{\tau lm'}|^2.
\end{aligned}$$

Here, all summations in m, m' and m'' are taken from $-l$ to l. Hence, L^2 is conserved under rotations as in the classical case. Note that this is also a symmetry operation for a sphere centered at the origin, which is reflected in an unchanged l-index truncation, see (2.5).

4.2 Invariants under translations

Upon a translation z along the z-axis, the far field amplitude $\boldsymbol{F}(\hat{\boldsymbol{r}}) \mapsto \boldsymbol{F}(\hat{\boldsymbol{r}})\mathrm{e}^{jkz\cos\theta}$. Since $\mathcal{L}_z = -\mathrm{j}\frac{\partial}{\partial\phi}$, it follows that upon the same translation, and for $\alpha = \theta$ or ϕ

$$\begin{aligned}
&[\mathcal{L}_z F_\alpha(\hat{\boldsymbol{r}})]^*\mathcal{L}_z F_\alpha(\hat{\boldsymbol{r}}) = \frac{\partial F_\alpha(\hat{\boldsymbol{r}})^*}{\partial\phi}\frac{\partial F_\alpha(\hat{\boldsymbol{r}})}{\partial\phi} \mapsto \\
&\frac{\partial}{\partial\phi}[F_\alpha(\hat{\boldsymbol{r}})^*\mathrm{e}^{-jkz\cos\theta}]\frac{\partial}{\partial\phi}[F_\alpha(\hat{\boldsymbol{r}})\mathrm{e}^{jkz\cos\theta}] = \frac{\partial F_\alpha(\hat{\boldsymbol{r}})^*}{\partial\phi}\frac{\partial F_\alpha(\hat{\boldsymbol{r}})}{\partial\phi}
\end{aligned}$$

Hence, L_z^2 is invariant under a translation along the z-axis. This is consistent with the classical symmetry for L_z^2. Moreover, a z-axis translation does not change the

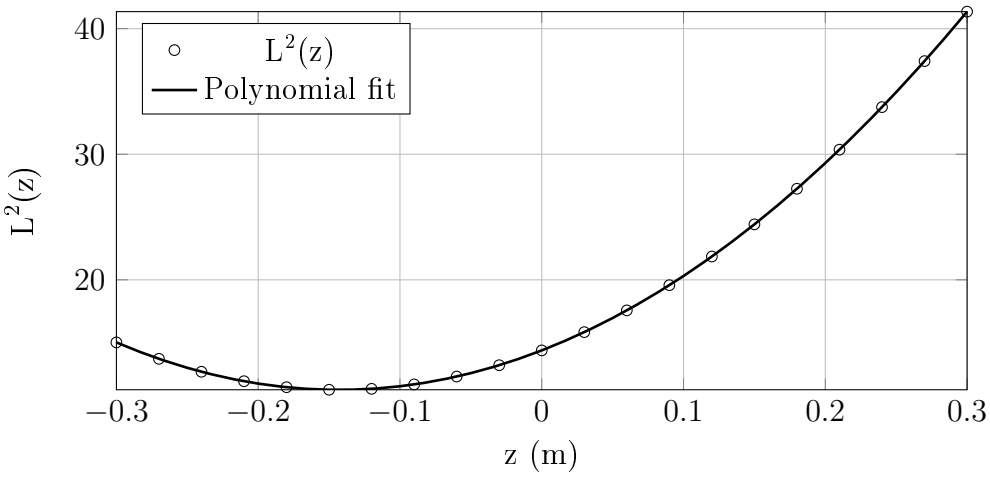

Figure 1: Illustration of the functional form of $L^2(z\hat{\boldsymbol{z}})$. The far field data for an antenna on a laptop computer is used, and L^2 was computed using translations and evaluation of L^2 using the SWE (2.6). A polynomial fit of degree 2 is depicted, which supports (4.1). A unique strict minimum is manifested for $L^2(z\hat{\boldsymbol{z}})$ at $z \approx -0.14$ m.

truncation limit of the m index (2.5). A justification of the mode truncation (2.5) can be derived as follows: consider an antenna current distribution in a circular disc of radius $\rho_{\min}$ in the xy-plane. The mode truncation of the corresponding SWE is $l \leq k\rho_{\min}+n$ and $|m| \leq k\rho_{\min}+n$. A translation of the current distribution to $z = z_0$ implies that the mode truncation changes to $l \leq k\sqrt{\rho_{\min}^2 + z_0^2} + n = kr_{\min} + n$ and $|m| \leq k\rho_{\min} + n$.

4.3 Translations

Let $L^2(\boldsymbol{d})$ be the angular momentum of a far field pattern $\boldsymbol{F}(\hat{\boldsymbol{r}})$ with the origin shifted the distance vector $\boldsymbol{d}$. By replacing $\boldsymbol{F}(\hat{\boldsymbol{r}}) \mapsto \boldsymbol{F}(\hat{\boldsymbol{r}})\mathrm{e}^{\mathrm{j}\boldsymbol{k}\cdot\boldsymbol{d}}$ and using (3.3) it follows, see App. C, that $L^2(\boldsymbol{d})$ is on the form

$$L^2(\boldsymbol{d}) = a_0 - 2k\boldsymbol{a}_1 \cdot \boldsymbol{d} + k^2 \boldsymbol{d} \cdot \mathbf{A}_2 \cdot \boldsymbol{d} \tag{4.1}$$

where a_0 is a real scalar, $\boldsymbol{a}_1$ is a real-valued vector, and $\boldsymbol{A}_2$ is a positive definite dyadic. For a numerical example, see Fig. 1. The explicit expressions are

$$\begin{cases} a_0 = L^2(\boldsymbol{F}(\hat{\boldsymbol{r}}), \mathbf{0}) = \displaystyle\iint_\Omega \boldsymbol{F}^*(\hat{\boldsymbol{r}}) \cdot \mathcal{L}^2 \boldsymbol{F}(\hat{\boldsymbol{r}}) \mathrm{d}\Omega, \\ \boldsymbol{a}_1 = \displaystyle\iint_\Omega \mathrm{Im}\left[F_\theta \nabla_\Omega F_\theta^* + F_\phi \nabla_\Omega F_\phi^*\right] \mathrm{d}\Omega - 2\iint_\Omega \cot\theta\, \mathrm{Im}(F_\theta F_\phi^*)\hat{\boldsymbol{\phi}} \mathrm{d}\Omega, \\ \mathbf{A}_2 = \displaystyle\iint_\Omega \boldsymbol{F}^*(\hat{\boldsymbol{r}}) \cdot \boldsymbol{F}(\hat{\boldsymbol{r}})[\hat{\boldsymbol{\theta}}\hat{\boldsymbol{\theta}} + \hat{\boldsymbol{\phi}}\hat{\boldsymbol{\phi}}] \mathrm{d}\Omega. \end{cases} \tag{4.2}$$

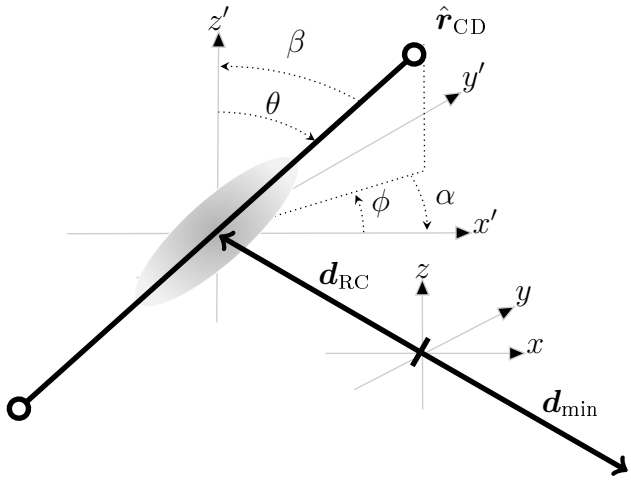

Figure 2: An antenna current distribution is depicted as a tilted ellipsoid, positioned at the *radiation center* $\boldsymbol{d}_{\mathrm{RC}}$ and with major axis along the *current distribution axis* $\hat{\boldsymbol{r}}_{\mathrm{CD}}$. The *current distribution axis* is indicated as a line ended by two circles. Two parallel coordinate systems are shown: the far field reference system xyz, and a parallel $x'y'z'$ system with origin at $\boldsymbol{d}_{\mathrm{RC}}$. The coordinate translation $\boldsymbol{d}_{\mathrm{min}} = -\boldsymbol{d}_{\mathrm{RC}}$ leading to minimum L^2 results in a centered antenna current (the ellipse) in the xyz system. A subsequent minimization of L_z^2 yields a rotation that aligns the antenna current (the ellipse) to the z-axis. This rotation can be decomposed in a first rotation $\alpha = -\phi$ around the $\hat{\boldsymbol{z}}$-axis, and a secondary rotation $\beta = -\theta$ around the y-axis.

See Appendix C for further details. It is noted that the Stokes parameter $s_3 = -2\,\mathrm{Im}(F_\theta F_\phi^*)$, measuring the power imbalance between left-handed and right-handed circular polarization, appears in the integral expression for $\boldsymbol{a}_1$. Note the formal equivalence with the classical result. Hence, there is a unique translation $\boldsymbol{d}_{\mathrm{min}}$ for which L^2 is minimized. The negative value of this translation vector is defined as the radiation center $\boldsymbol{d}_{\mathrm{RC}}$ in the coordinate system in which the far field pattern is given, see Fig. 2.

By using (4.1) and $\mathbf{A}_2^T = \mathbf{A}_2$, the radiation center can be written as

$$\boldsymbol{d}_{\mathrm{RC}} = -\boldsymbol{d}_{\mathrm{min}} = -\frac{1}{k}\mathbf{A}_2^{-1} \cdot \boldsymbol{a}_1. \tag{4.3}$$

This minima is unique, since $\mathbf{A}_2$ is positive definite. This fact is proved in Appendix C. Notice that finding the minimizer only involves elementary matrix algebra, once the vector $\boldsymbol{a}_1$ and the matrix $\mathbf{A}_2$ are found.

Moreover, since $L^2(\boldsymbol{d})$ is a second order polynomial in $\boldsymbol{d}$, it suffices to calculate three samples of $L^2(\boldsymbol{d})$ along each of the three coordinate axes in order to fully characterize $L^2(\boldsymbol{d})$.

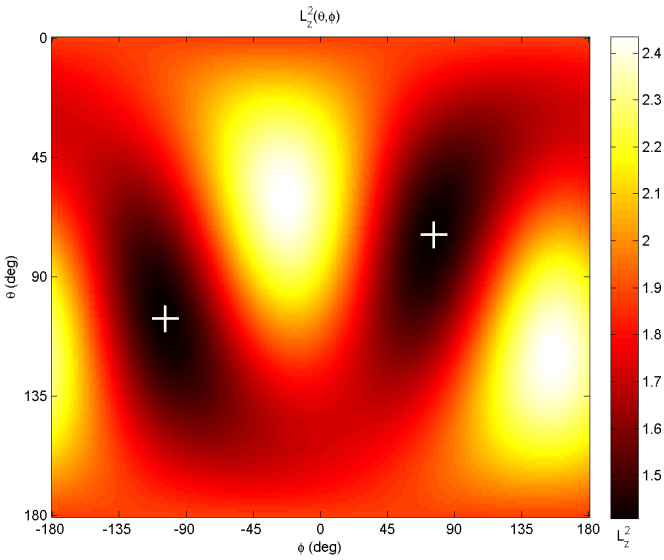

Figure 3: Illustration of the functional form of $L_z^2(\hat{\boldsymbol{r}}(\theta,\phi))$, where spherical coordinates are used (A.1), and the angles of rotation are $\beta = -\theta$ and $\gamma = -\phi$. The far field data for an antenna on a laptop computer is used. Two directions, corresponding to the minimum of L_z^2, are marked with white crosses. These directions are spatially reversed, which is clearly visible in the polar plot of the same data, see Fig. 4.

4.4 Rotations

The invariance under rotation of L^2 was investigated in Section 4.1. In this section, the rotational properties of L_z^2 are analyzed.

Consider an arbitrary rotation defined as a $z-y-z$ Euler rotation with rotation angles α, β, and γ, respectively. The initial α rotation around the z-axis merely changes the phase of the mode amplitudes [4], and, hence, L_z^2 is a function of β and γ only. Due to spatial reversal symmetry, we also have

$$L_z^2(\pi-\beta,\gamma+\pi) = L_z^2(\beta,\gamma).$$

From this relation we conclude that it suffices to investigate the upper part of the unit sphere, $\beta \in [0,\pi/2]$, $\gamma \in [-\pi,\pi)$, for minima. Since $L_z^2(\beta,\gamma)$ is a continuous function in the angles β and γ, the minimum of the function is obtained, but it might not be unique. If the minimum is unique, (β_0,γ_0), then the inverse rotation, $(\beta_0,\pi-\gamma_0)$, of $\hat{\boldsymbol{z}}$ defines the current distribution axis $\hat{\boldsymbol{r}}_{\mathrm{CD}}$. Note, that a minimum also occurs in the spatially reversed direction. In Figs 3 and 4 the functional form of L_z^2 is depicted with respect to rotations around the radiation center of an antenna on a laptop computer. The angles θ and ϕ in the Fig. 3 are related to the rotation as $\beta = -\theta$ and $\gamma = -\phi$.

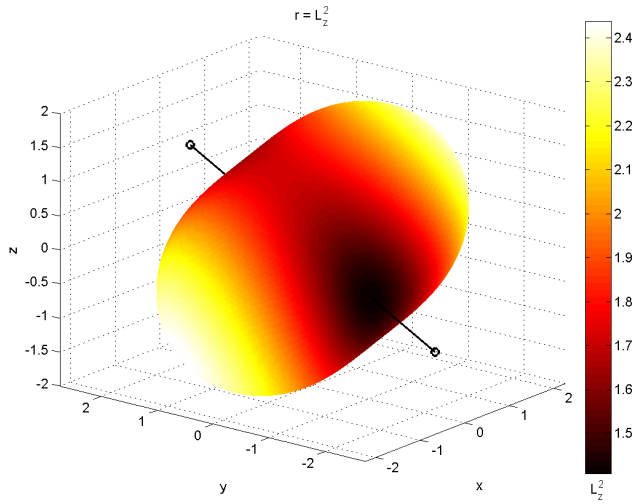

Figure 4: Polar plot of $L_z^2(\hat{\boldsymbol{r}})$, for an antenna on a laptop computer, see Fig 5. The *current distribution axis* is depicted as a line ended by two circles.

5 Examples

Calculations of *radiation center* and *current distribution axis* are made for a number of antennas. The antennas are chosen to demonstrate the capability of the proposed method, and its applicability for any antenna type. In these examples, the current distribution is that of an embedded far field pattern, *i.e.*, one antenna port is fed, while the other ports are terminated in matched loads.

A laptop and a cellular phone are designed for MIMO capacity with no explicit design criteria for the radiation pattern or polarization state. On the other hand, in the examples with a base station antenna and a cylindrical array antenna, the antennas are designed for a given radiation pattern, with main lobe and side lobe regions, and a given polarization state.

In the examples, the exact mounting of the radiating device was not specified in the measurement data. Instead, the radiation centers were calculated and far field data was translated to fit the first antenna port. Note that the proposed method provides a method to estimate the mounting position of the radiating device, and the method works for any type of antenna.

The coordinate transformations involved in the numerical algorithm are depicted in Fig. 2. The numerical algorithm, used to calculate the *radiation center* $\boldsymbol{d}_{\mathrm{RC}}$ and the *current distribution axis* $\hat{\boldsymbol{r}}_{\mathrm{CD}}$, is outlined here:

1. Find the point $\boldsymbol{d}_{\min}$ that minimizes $L^2(\boldsymbol{d})$.

2. Calculate the *radiation center* $\boldsymbol{d}_{\mathrm{RC}} = -\boldsymbol{d}_{\min}$.

3. Translate the far field by $\boldsymbol{d}_{\min}$: $\boldsymbol{F}(\hat{\boldsymbol{r}}) \mapsto \boldsymbol{F}(\hat{\boldsymbol{r}})\mathrm{e}^{\mathrm{j}\boldsymbol{k}\cdot\boldsymbol{d}_{\min}}$.

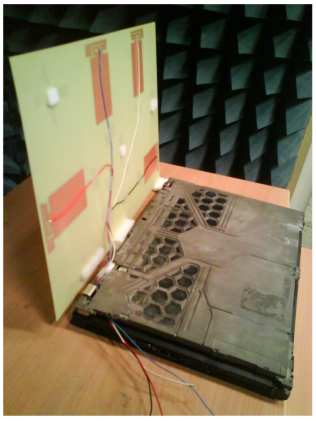

Figure 5: Photo of the laptop equipped with four antennas.

4. Find the rotation $\mathbf{R}$ that minimizes L_z^2.
5. The *current distribution axis* points along $\hat{\boldsymbol{r}}_{\mathrm{CD}} = \mathbf{R}^{-1} \cdot \hat{\boldsymbol{z}}$.

In Figs 1 and 3 the functional form of $L^2(\boldsymbol{d})$ and $L_z^2(\hat{r})$ are depicted for an antenna on a laptop computer, see Sec. 5.1.

5.1 Antennas on a laptop

In the first example, a laptop mock-up with four antennas on the lid is considered, see Fig. 5. The measured far field data was used as input to the algorithm, and the radiation center and the current distribution axis were calculated for all ports at 750 MHz frequency. The result is depicted in Fig. 6. For the first three antennas, the radiation centers are in the plane of the lid whereas for the rightmost antenna the radiation center is located slightly off the lid. The explanation for this could be radiation from the connecting cables or a measurement impairment such as turn table blocking, or reflections in the keyboard.

The antennas of the laptop are designed and optimized for low correlation. An effect of this optimization is the almost perpendicular current distributions axes of the two top antennas (no 2 and 3).

5.2 Antennas on a cellular phone

In this example, we consider a cellular phone, see Fig. 7, equipped with four antenna elements. The computed radiation centers and the current distributions axes are depicted in Fig. 8. The radiation centers are distributed quite symmetrically and slightly inside the antennas. This effect is most probably due to the antenna function, that acts as a probe setting up currents on the antenna chassis. Any impairments of connecting cables seem to be low. The sphericity is quite high as expected for electrically small antennas.

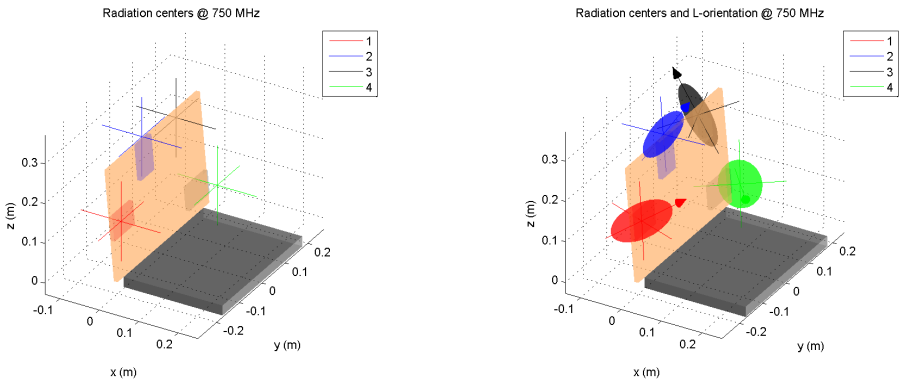

Figure 6: Radiation center $\boldsymbol{d}_{\mathrm{RC}}$ (left) and current distributions axes $\hat{\boldsymbol{r}}_{\mathrm{CD}}$ (right) for four antennas on a laptop. The axial ratio of the ellipses indicate the sphericity (2.7) of the current distribution.

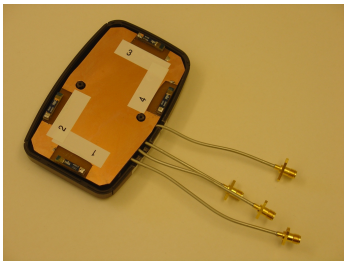

Figure 7: Photo of the cellular phone equipped with four antennas.

5.3 Columns of a base station antenna

A mobile base station antenna consists of four horizontally distributed columns each equipped with doubly polarized elements with 45 degree slanted co-polarizations, as shown in Fig. 9. This antenna was purchased and investigated for beam forming and MIMO capacity. The zig-zag pattern between the radiation centers of the antenna columns were later confirmed by dis-mounting the antenna radome.

As expected, a low sphericity is found for the elongated antenna columns. Note that the current distribution for each port consists of the total current on all antenna elements in a vertical antenna column. Clearly, the results show that the antenna currents are vertical. Another interesting note is that the sphericity is slightly higher for the outer columns.

5.4 Elements of a cylindrical array antenna

In a final example, we show a 64 element cylindrical array antenna with dual polarized vertical/horizontal elements, and designed for the band 2.5–2.6 GHz. The antenna element is a dual stacked patch, and the element separation is 58 mm, *i.e.*, $\lambda/2$ mm at 2.6 GHz, both in the vertical and the horizontal direction. Embedded

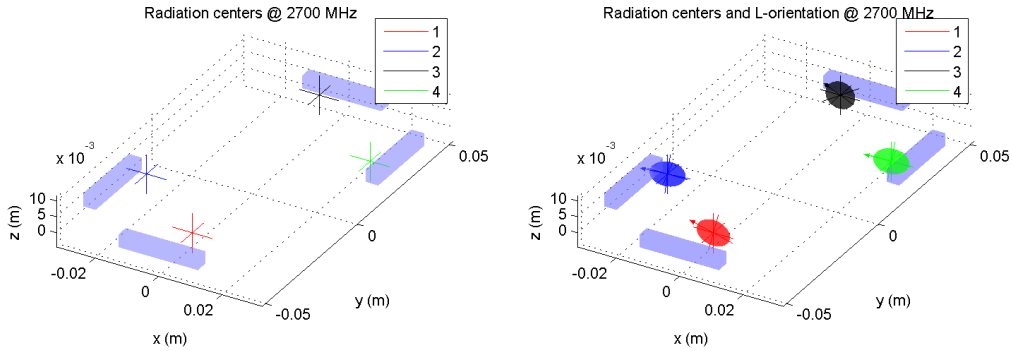

Figure 8: Radiation centers and current distributions axes for four antennas on a cellular phone. The axial ratios of the ellipses indicate the sphericity (2.7) of the current distribution.

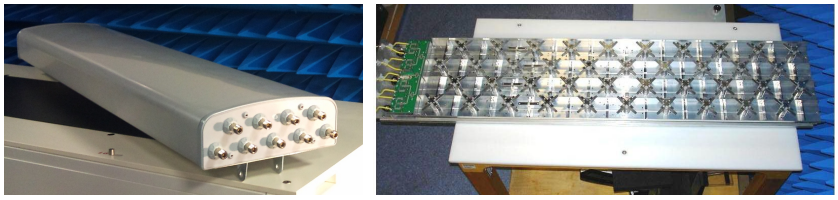

Figure 9: Photos of the base station antenna with (left) and without (right) radome. The antenna is equipped with eight antenna ports for the four columns of dual polarized antenna elements. The ninth port is used for electrical tilt control. In the right photo it can be seen that the neighboring columns are shifted in a zig-zag pattern.

far field patterns at 2.5 GHz for all the 128 antenna ports were used as input to the algorithm. The array antenna is depicted in Fig. 11, and the radiation centers for both polarizations and all 64 elements were calculated. The result is depicted in Figs 12, 13, and 14. Measurement impairments can be identified for at least two elements in the bottom row, *i.e.*, the row closest to the turn table. The results for the vertical and horizontal antenna polarization are very similar. Therefore, only results for the vertical polarization are shown.

6 Conclusions

A new method to investigate the sources of radiation of an antenna has been introduced. The method provides a unique position and orientation of the antenna currents. Solid proofs are provided that guarantee that the output of the algorithm is unique. The underlying theory is based on the quantum mechanical definition of angular momentum. In addition, the used cost functions L^2 and L_z^2 are shown to be of a simple shape, which can be used for efficient implementation of the numerical

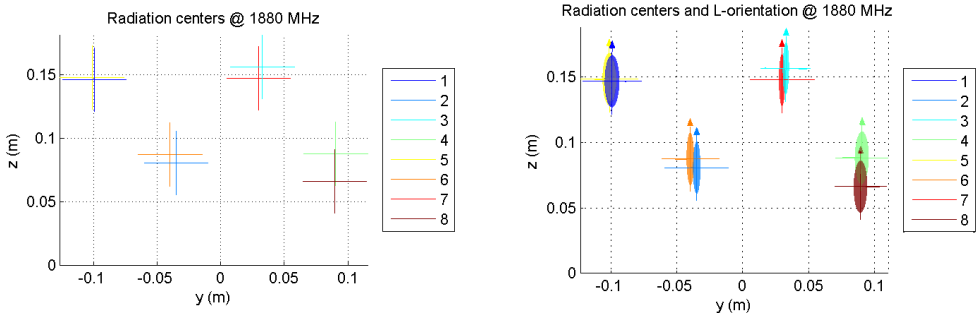

Figure 10: Radiation centers (left) and current distributions axes (right) for the eight antenna ports of the base station antenna. The axial ratios of the ellipses indicate the sphericity (2.7) of the current distributions, which in this case is low due to the large height-to-width ratio of each antenna column. For each antenna port, a column of 10 antenna elements, of either $+45°$ or $-45°$ slanted linear polarization, are fed.

algorithm. Very small deviations between the numerical cost functions and the theoretical ones, have been observed. These deviations are most probably due to the finite truncation of the SWE.

The underlying cost functions are defined using the mode amplitudes $a_{\tau lm}$ of the SWE of the far field, see (2.6). However, equivalent definitions are given in terms of the far field, see (3.3) and (3.4). Hence, a numerical algorithm can be carried out either using the mode amplitudes $a_{\tau lm}$ or the far field amplitudes $\boldsymbol{F}(\hat{\boldsymbol{r}})$. In this paper, the results are based on translation and rotation of mode amplitudes. Note that, apart from a tool for rotations and translations of the far field, only elementary mathematical operations are needed.

Calculation of the x and y components of $\boldsymbol{a}_1$ involve a $\sin\theta$ singularity which causes numerical instability. A numerical robust solution is obtained by rotating the far field amplitude $-\pi/2$ around the y-axis and use $\boldsymbol{a}_1 \cdot \hat{z}$ for the rotated far field to calculate $\boldsymbol{a}_1 \cdot \hat{x}$ for the un-rotated far field, see Appendix C. For the y-component a rotation $\pi/2$ around the x-axis can be used.

Compared to standard calculation of phases center [1], no decisions have to be made on which polarization component and angular region to use. The required input is a full sphere radiation pattern, which inherently defines the antenna polarization. Regions of non-significant radiation are naturally suppressed by the low values of the far field magnitudes. Results of the algorithm has been shown for four different types of antennas with no changes in parameter settings. Note that the method works for any antenna type and any antenna element geometry.

In the case of planar cuts of complex far field data, a similar approach can be used. In this case, the basis functions can be taken as $\exp(jm\alpha)$ for integer m, where α is the periodic angle of the cut. A radiation center corresponding to the far field data in the planar cut can then be obtained by minimizing $\sum_{p,m} m^2 |a_{p,m}|^2$ versus

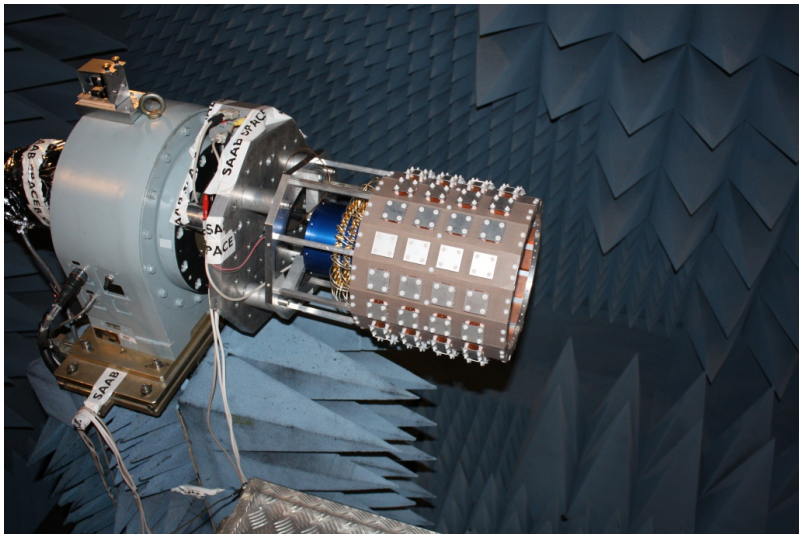

Figure 11: Photo of the cylindrical array antenna, with 64 dual-polarized antenna patch elements on a faceted ground plane, mounted on the turn table.

translations in the plane. Here $a_{p,m}$ are the expansion coefficients for polarization p and basis function m.

Acknowledgement

This work has been carried out by support from Ericsson AB, which is gratefully acknowledged.

Appendix A Vector spherical harmonics

The vector spherical harmonics $\boldsymbol{A}_{\tau lm}(\hat{\boldsymbol{r}})$ for $\tau = 1, 2$, $l = 1, 2, \ldots, \infty$, $m = -l, -l+1, \ldots, l$ used in this paper are defined as

$$\begin{cases} \boldsymbol{A}_{1lm}(\hat{\boldsymbol{r}}) = \dfrac{1}{\sqrt{l(l+1)}} \nabla Y_{lm}(\hat{\boldsymbol{r}}) \times \boldsymbol{r} \\ \boldsymbol{A}_{2lm}(\hat{\boldsymbol{r}}) = \dfrac{1}{\sqrt{l(l+1)}} r \nabla Y_{lm}(\hat{\boldsymbol{r}}) \end{cases}$$

The spherical harmonics, $Y_{lm}(\theta, \phi)$, are defined by

$$Y_{lm}(\theta, \phi) = \sqrt{\frac{2l+1}{4\pi} \frac{(l-m)!}{(l+m)!}} P_l^m(\cos\theta) \mathrm{e}^{\mathrm{j}m\phi}.$$

and the spherical coordinates (r, θ, ϕ) are defined as

$$\boldsymbol{r} = x\hat{\boldsymbol{x}} + y\hat{\boldsymbol{y}} + z\hat{\boldsymbol{z}} = \sin\theta(\cos\phi\hat{\boldsymbol{x}} + \sin\phi\hat{\boldsymbol{y}}) + \cos\theta\hat{\boldsymbol{z}}. \tag{A.1}$$

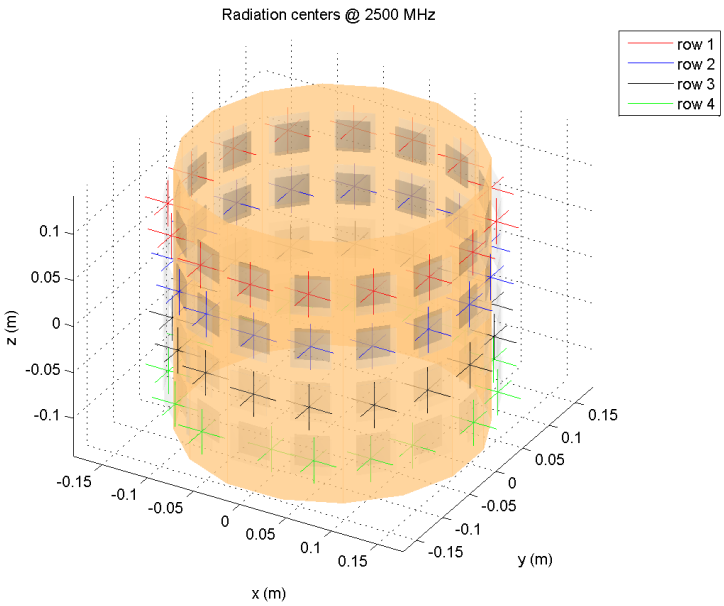

Figure 12: Radiation centers for the 64 element cylindrical array equipped using embedded far field patterns for the vertically polarized antenna ports. The radiation centers are depicted as three-dimensional crosses, and colored row by row. A pair of stacked patches, for each antenna element, are depicted as gray squares. The outer patch is slightly larger than the inner.

The vector spherical harmonics (and the spherical harmonics) are orthonormal on the unit sphere Ω,

$$\iint_{\Omega} \boldsymbol{A}_{\tau lm}(\hat{\boldsymbol{r}}) \cdot \boldsymbol{A}_{\tau' l' m'}(\hat{\boldsymbol{r}}) \, \mathrm{d}\Omega = \delta_{\tau\tau'}\delta_{mm'}\delta_{ll'} \tag{A.2}$$

and

$$\iint_{\Omega} Y_{lm}(\hat{\boldsymbol{r}}) Y_{l'm'}(\hat{\boldsymbol{r}}) \, \mathrm{d}\Omega = \delta_{ll'}\delta_{mm'}$$

The angular momentum of a far field is a dyadic quantity. In spherical coordinates the representation of the angular momentum operator on a transverse vector field $\boldsymbol{F}(\hat{\boldsymbol{r}})$ is

$$\begin{aligned}\mathcal{L}\boldsymbol{F} &= -\mathrm{j}\boldsymbol{r} \times \nabla \boldsymbol{F} \\ &= -\mathrm{j}\hat{\boldsymbol{\theta}} \frac{1}{\sin\theta} \left(\hat{\boldsymbol{r}} \sin\theta F_\phi + \hat{\boldsymbol{\theta}} \left(\cos\theta F_\phi - \frac{\partial F_\theta}{\partial \phi} \right) - \hat{\boldsymbol{\phi}} \left(\cos\theta F_\theta + \frac{\partial F_\phi}{\partial \phi} \right) \right) \\ &\quad - \mathrm{j}\hat{\boldsymbol{\phi}} \left(-\hat{\boldsymbol{r}} F_\theta + \hat{\boldsymbol{\theta}} \frac{\partial F_\theta}{\partial \theta} + \hat{\boldsymbol{\phi}} \frac{\partial F_\phi}{\partial \theta} \right).\end{aligned} \tag{A.3}$$

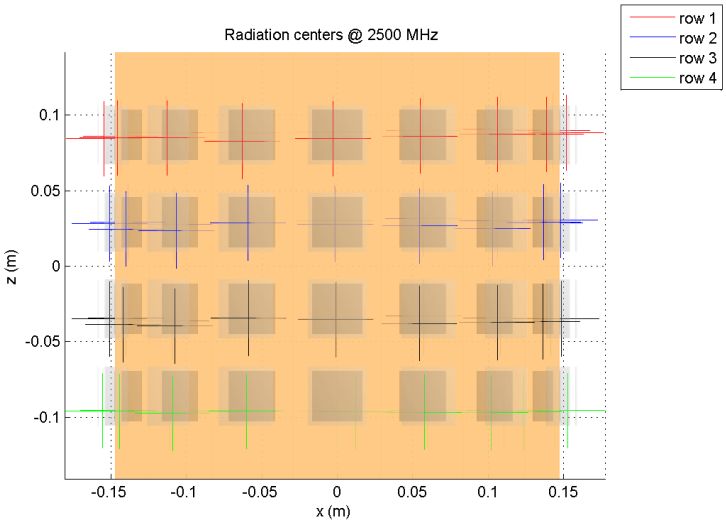

Figure 13: Side view of radiation centers depicted in Fig 12. The radiation centers are slightly more separated than the mechanical separation of the antenna elements. This could be an effect of mutual coupling.

The angular parts of the nabla and the Laplace operators are

$$\begin{cases} \nabla_\Omega = r\mathbf{P}_\Omega \cdot \nabla = \hat{\boldsymbol{\theta}}\dfrac{\partial}{\partial\theta} + \hat{\boldsymbol{\phi}}\dfrac{1}{\sin\theta}\dfrac{\partial}{\partial\phi}, \\ \nabla_\Omega^2 = \dfrac{1}{\sin\theta}\dfrac{\partial}{\partial\theta}\left(\sin\theta\dfrac{\partial}{\partial\theta}\right) + \dfrac{1}{\sin^2\theta}\dfrac{\partial^2}{\partial\phi^2} \end{cases}$$

where $P_\Omega = \mathbf{I} - \hat{\boldsymbol{r}}\hat{\boldsymbol{r}}$ is the projection operator on the unit sphere. The explicit form of the $\mathcal{P}_\Omega\mathcal{L}^2$ operator acting on a transverse vector field on the unit sphere is [2]

$$\begin{aligned} \mathcal{P}_\Omega\mathcal{L}^2\boldsymbol{F}(\hat{\boldsymbol{r}}) =& \hat{\boldsymbol{\theta}}\left(-\nabla_\Omega^2 F_\theta + \frac{F_\theta}{\sin^2\theta} + \frac{2\cos\theta}{\sin^2\theta}\frac{\partial F_\phi}{\partial\phi}\right) \\ & \hat{\boldsymbol{\phi}}\left(-\nabla_\Omega^2 F_\phi + \frac{F_\phi}{\sin^2\theta} - \frac{2\cos\theta}{\sin^2\theta}\frac{\partial F_\theta}{\partial\phi}\right) \end{aligned} \tag{A.4}$$

The spherical harmonics $Y_{lm}(\hat{\boldsymbol{r}})$ are eigenfunctions of $\mathcal{L}^2$

$$\mathcal{L}^2 Y_{lm}(\hat{\boldsymbol{r}}) = l(l+1)Y_{lm}(\hat{\boldsymbol{r}})$$

The corresponding relations for the vector spherical harmonics are [6, pp. 1900–01]

$$\begin{cases} \mathcal{P}_\Omega\mathcal{L}^2\boldsymbol{A}_{1lm}(\hat{\boldsymbol{r}}) = \mathbf{P}_\Omega \cdot l(l+1)\boldsymbol{A}_{1lm}(\hat{\boldsymbol{r}}) = l(l+1)\boldsymbol{A}_{1lm}(\hat{\boldsymbol{r}}), \\ \mathcal{P}_\Omega\mathcal{L}^2\boldsymbol{A}_{2lm}(\hat{\boldsymbol{r}}) = \mathbf{P}_\Omega \cdot [l(l+1)\boldsymbol{A}_{2lm}(\hat{\boldsymbol{r}}) - 2\sqrt{l(l+1)}Y_{lm}(\hat{\boldsymbol{r}})\hat{\boldsymbol{r}}] = l(l+1)\boldsymbol{A}_{2lm}(\hat{\boldsymbol{r}}) \end{cases}$$

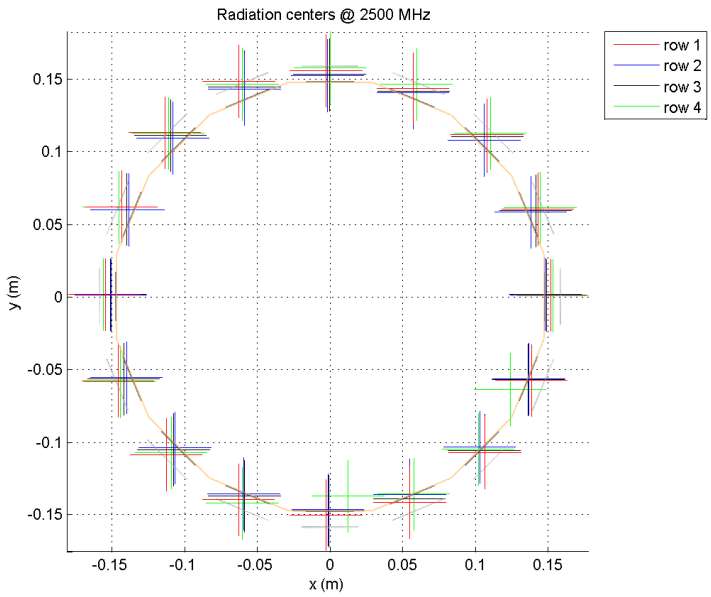

Figure 14: Top view of the radiation centers depicted in Fig. 12. The radiation centers are located slightly behind the top patch of the antenna elements. Moreover, two elements in the bottom row, at appr. 6 and 4 o'clock, suffer from measurement impairments, resulting in a radiation center inside the cylindrical ground plane.

Any transverse component of $\boldsymbol{A}_{\tau lm}$ has ϕ-dependence $\exp(\mathrm{j}m\phi)$ and is hence an eigenfunction of $\mathcal{L}_z$.

Appendix B Product rules for angular momentum

Let $\Phi(\theta,\phi)$ and $\Psi(\theta,\phi)$ be two scalar fields that do not depend on r. Standard differentiation rules then gives the identity

$$\mathcal{L}^2(\Phi\Psi) = -\nabla_\Omega^2(\Phi)\Psi - \Phi\nabla_\Omega^2(\Psi) - 2\nabla_\Omega\Phi\cdot\nabla_\Omega\Psi \tag{B.1}$$

The following product then follows from (B.1) and (A.4)

$$\begin{aligned}\mathcal{P}_\Omega\mathcal{L}^2(\boldsymbol{F}\Psi) &= (\mathcal{P}_\Omega\mathcal{L}^2\boldsymbol{F})\Psi + \boldsymbol{F}(\mathcal{L}^2\Psi)\\ &- 2\left[\hat{\boldsymbol{\theta}}\nabla_\Omega F_\theta + \hat{\boldsymbol{\phi}}\nabla_\Omega F_\phi\right]\cdot\nabla_\Omega\Psi - 2\frac{\cos\theta}{\sin^2\theta}(\hat{\boldsymbol{r}}\times\boldsymbol{F})\frac{\partial\Psi}{\partial\phi}\end{aligned} \tag{B.2}$$

Appendix C Translational properties of the angular momentum

The angular momentum or L^2 changes when the far field is translated. A general translation along $\boldsymbol{d}$ generates the phase shift

$$\boldsymbol{F}(\hat{\boldsymbol{r}}) \mapsto \boldsymbol{F}(\hat{\boldsymbol{r}})\mathrm{e}^{j\boldsymbol{k}\cdot\boldsymbol{d}}.$$

The square of the angular momentum is thus calculated as

$$L^2(\boldsymbol{F}(\hat{\boldsymbol{r}}), \boldsymbol{d}) = \iint_\Omega \boldsymbol{F}^*(\hat{\boldsymbol{r}})\mathrm{e}^{-j\boldsymbol{k}\cdot\boldsymbol{d}} \cdot \mathcal{P}_\Omega \mathcal{L}^2 \boldsymbol{F}(\hat{\boldsymbol{r}})\mathrm{e}^{j\boldsymbol{k}\cdot\boldsymbol{d}}\mathrm{d}\Omega. \tag{C.1}$$

Since $\mathcal{L}^2$ contains second order derivatives in θ and ϕ, and lower order terms, it is straightforward to show that the squared angular momentum is a second order polynomial in $\boldsymbol{d}$.

Now (B.2) is used with $\Psi = \exp(j\boldsymbol{k}\cdot\boldsymbol{d}) = \exp(jk\hat{\boldsymbol{r}}\cdot\boldsymbol{d})$. The derivatives of Ψ then become

$$\begin{cases} \dfrac{\partial\Psi}{\partial\theta} = jk\hat{\boldsymbol{\theta}}\cdot\boldsymbol{d}\mathrm{e}^{j\boldsymbol{k}\cdot\boldsymbol{d}}, \\ \dfrac{\partial\Psi}{\partial\phi} = jk\hat{\boldsymbol{\phi}}\cdot\boldsymbol{d}\sin\theta\mathrm{e}^{j\boldsymbol{k}\cdot\boldsymbol{d}}, \\ \nabla_\Omega\Psi = jk\left[\hat{\boldsymbol{\theta}}\hat{\boldsymbol{\theta}} + \hat{\boldsymbol{\phi}}\hat{\boldsymbol{\phi}}\right]\cdot\boldsymbol{d}\mathrm{e}^{j\boldsymbol{k}\cdot\boldsymbol{d}}, \\ \mathcal{L}^2[\Psi] = j2k\hat{\boldsymbol{r}}\cdot\boldsymbol{d}\mathrm{e}^{j\boldsymbol{k}\cdot\boldsymbol{d}} + k^2\left[(\hat{\boldsymbol{\theta}}\cdot\boldsymbol{d})^2 + (\hat{\boldsymbol{\phi}}\cdot\boldsymbol{d})^2\right]\mathrm{e}^{j\boldsymbol{k}\cdot\boldsymbol{d}}. \end{cases} \tag{C.2}$$

Using (B.2) and (C.2) in (C.1) then leads to

$$L^2[\boldsymbol{F}(\hat{\boldsymbol{r}}), \boldsymbol{d}] = a_0 - 2k\boldsymbol{a}_1\cdot\boldsymbol{d} + k^2\boldsymbol{d}\cdot\mathbf{A}_2\cdot\boldsymbol{d} \tag{C.3}$$

where

$$\begin{cases} a_0 = L^2(\boldsymbol{F}(\hat{\boldsymbol{r}}), \mathbf{0}) = \iint_\Omega \boldsymbol{F}^*(\hat{\boldsymbol{r}})\cdot\mathcal{L}^2\boldsymbol{F}(\hat{\boldsymbol{r}})\mathrm{d}\Omega, \\ \boldsymbol{a}_1 = -\mathrm{j}\iint_\Omega \boldsymbol{F}^*(\hat{\boldsymbol{r}})\cdot\boldsymbol{F}(\hat{\boldsymbol{r}})\hat{\boldsymbol{r}}\mathrm{d}\Omega + \mathrm{j}\iint_\Omega \left[F_\theta^*\nabla_\Omega F_\theta + F_\phi^*\nabla_\Omega F_\phi\right]\mathrm{d}\Omega \\ \qquad + \mathrm{j}\iint_\Omega \cot\theta\hat{\boldsymbol{r}}\cdot(\boldsymbol{F}(\hat{\boldsymbol{r}})\times\boldsymbol{F}^*(\hat{\boldsymbol{r}}))\hat{\boldsymbol{\phi}}\mathrm{d}\Omega \\ \mathbf{A}_2 = \iint_\Omega \boldsymbol{F}^*(\hat{\boldsymbol{r}})\cdot\boldsymbol{F}(\hat{\boldsymbol{r}})[\hat{\boldsymbol{\theta}}\hat{\boldsymbol{\theta}} + \hat{\boldsymbol{\phi}}\hat{\boldsymbol{\phi}}]\mathrm{d}\Omega. \end{cases} \tag{C.4}$$

All quantities in (C.4) are real-valued. To see this, $\boldsymbol{a}_1$ is further simplified by applying the Gauss theorem on the unit sphere [8, Eq. (A3.45)]

$$\iint_\Omega u(\hat{\boldsymbol{r}})\hat{\boldsymbol{r}}\mathrm{d}\Omega = \frac{1}{2}\iint_\Omega \nabla_\Omega u(\hat{\boldsymbol{r}})\mathrm{d}\Omega.$$

Moreover, $\mathrm{j}\hat{\boldsymbol{r}}\cdot(\boldsymbol{F}\times\boldsymbol{F}^*) = -2\,\mathrm{Im}\,F_\theta F_\phi^*$. Hence, the linear term can be written as

$$\boldsymbol{a}_1 = \iint_\Omega \mathrm{Im}\left[F_\theta \nabla_\Omega F_\theta^* + F_\phi \nabla_\Omega F_\phi^*\right] \mathrm{d}\Omega - 2\iint_\Omega \cot\theta\, \mathrm{Im}(F_\theta F_\phi^*)\hat{\boldsymbol{\phi}}\mathrm{d}\Omega.$$

Straightforward differentiation of (C.3) leads to the following expression for the radiation center, *i.e.*, the negative of the point where the minimum of L^2 is obtained,

$$\boldsymbol{d}_{\mathrm{RC}} = -\boldsymbol{d}_{\min} = -\frac{1}{k}\mathbf{A}_2^{-1} \cdot \boldsymbol{a}_1.$$

For any vector $\boldsymbol{d} = d\hat{\boldsymbol{d}}$, the quadratic term

$$\boldsymbol{d} \cdot \mathbf{A}_2 \cdot \boldsymbol{d} = d^2 \iint_\Omega \boldsymbol{F}^* \cdot \boldsymbol{F}[(\hat{\boldsymbol{d}} \cdot \hat{\boldsymbol{\theta}})^2 + (\hat{\boldsymbol{d}} \cdot \hat{\boldsymbol{\phi}})^2]\mathrm{d}\Omega > 0.$$

Hence, $\mathbf{A}_2$ is a positive definite matrix, which guarantees that the radiation center is uniquely defined.

For translations along the z-axis, $\boldsymbol{d} = z\hat{\boldsymbol{z}}$ and

$$L^2[\boldsymbol{F}(\hat{\boldsymbol{r}}), z\hat{\boldsymbol{z}}] = a_0 - 2k\boldsymbol{a}_1 \cdot \hat{\boldsymbol{z}}z + k^2z^2\hat{\boldsymbol{z}} \cdot \mathbf{A}_2 \cdot \hat{\boldsymbol{z}}, \tag{C.5}$$

where

$$\begin{cases} \boldsymbol{a}_1 \cdot \hat{\boldsymbol{z}} = \displaystyle\iint_\Omega \mathrm{Im}\left(F_\theta \frac{\partial F_\theta^*}{\partial\theta} + F_\phi \frac{\partial F_\phi^*}{\partial\theta}\right)\mathrm{d}\Omega \\ \hat{\boldsymbol{z}} \cdot \mathbf{A}_2 \cdot \hat{\boldsymbol{z}} = \displaystyle\iint_\Omega \boldsymbol{F}^*(\hat{\boldsymbol{r}}) \cdot \boldsymbol{F}(\hat{\boldsymbol{r}}) \sin^2\theta \mathrm{d}\Omega. \end{cases}$$

For square integrable far field amplitudes with non-zero norm, it then follows that $\hat{\boldsymbol{z}} \cdot \mathbf{A}_2 \cdot \hat{\boldsymbol{z}} > 0$ and hence $L^2[\boldsymbol{F}(\hat{\boldsymbol{r}}), z\hat{\boldsymbol{z}}]$ must have a strict local minimum at

$$z_{\min} = \frac{1}{k}\frac{\boldsymbol{a}_1 \cdot \hat{\boldsymbol{z}}}{\hat{\boldsymbol{z}} \cdot \mathbf{A}_2 \cdot \hat{\boldsymbol{z}}}.$$

Appendix D Angular momentum of dipole modes

For comparison and testing purposes, the angular momentum of the dipole modes ($l = 1$) is given in this appendix.

Any single mode field has its radiation center at the origin and hence $\boldsymbol{a}_1$ of (C.4) is zero. By the symmetry between electrical and magnetic modes (TM/TE), the results in this appendix applies to either electric or magnetic modes.

A translated z-dipole ($l = 1$, $m = 0$) has a squared angular momentum given by

$$L^2(\boldsymbol{A}_{\tau 10}, \boldsymbol{r}) = 2 + \frac{3}{5}(kx^2 + ky^2) + \frac{4}{5}kz^2 \tag{D.1}$$

and for the modes $l = 1$, $m = \pm 1$

$$L^2(\boldsymbol{A}_{\tau 1\pm 1}, \boldsymbol{r}) = 2 + \frac{7}{10}(kx^2 + ky^2) + \frac{3}{5}kz^2.$$

The odd/even modes

$$\boldsymbol{A}_{\tau,1,\mathrm{odd/even}} = (\boldsymbol{A}_{\tau 11} \mp \boldsymbol{A}_{\tau 1-1})/\sqrt{2}$$

correspond to dipoles directed along the x- and y-axis, respectively. The corresponding squared angular momenta for the translated far fields are

$$\begin{cases} L^2(\boldsymbol{A}_{\tau 1\mathrm{odd}}, \boldsymbol{r}) = 2 + \frac{3}{5}(ky^2 + kz^2) + \frac{4}{5}kx^2, \\ L^2(\boldsymbol{A}_{\tau 1\mathrm{even}}, \boldsymbol{r}) = 2 + \frac{3}{5}(kz^2 + kx^2) + \frac{4}{5}ky^2. \end{cases}$$

as expected by permutation of the x, y, and z-axes.

References

[1] IEEE145-1993. IEEE standard definition of terms for antennas, March 1993.

[2] G. Arfken. *Mathematical Methods for Physicists.* Academic Press, Orlando, third edition, 1985.

[3] A. R. Edmonds. *Angular Momentum in Quantum Mechanics.* Princeton, 3rd edition, 1974.

[4] J. Hald, J. E. Hansen, F. Jensen, and F. Holm Larsen. *Spherical Near-Field Antenna Measurements*, volume 26 of *IEE electromagnetic waves series.* Peter Peregrinus Ltd., 1998. edited by J.E. Hansen.

[5] F. Jensen and A. Frandsen. On the number of modes in spherical wave expansions. Technical report, TICRA, TICRA, Læderstræde 34, DK-1201 Copenhagen, Denmark, 2009.

[6] P. M. Morse and H. Feshbach. *Methods of Theoretical Physics*, volume 2. McGraw-Hill, New York, 1953.

[7] J. J. Sakurai. *Modern Quantum Mechanics.* Addison Wesley, 1985.

[8] J. G. Van Bladel. *Electromagnetic Fields.* IEEE Press, Piscataway, NJ, second edition, 2007.